Removal of acid red 151 dye from water by iron-impregnated heat treated egg shell bio-adsorbent

Elmira Moaveni[a], Elham Keshmirizadeh[a,*], Hamid Modarress[b]

[a]*Department of Chemistry, Karaj Branch, Islamic Azad University, P.O. Box 31485-313, Karaj, Iran, Tel. +98 26 34182305;*
Fax: +98 26 34418156; email: keshmiri@kiau.ac.ir (E. Keshmirizadeh), Tel. +98 26 34182318; email: elmira.moaveni@gmail.com (E. Moaveni)
[b]*Department of Chemical Engineering, Amir-Kabir University of Technology, No. 424, Hafez Avenue, P.O. Box 15875-4413, Tehran, Iran, Tel. +98 21 6454 3176; Fax: +98 21 66405847; email: hmodares@aut.ac.ir*

abstract

Acid red 151 (AR151) dye adsorption on iron-impregnated heat treated egg shell (Fe-HTES) with $FeCl_2$, $Fe(NO_3)_3$ and K_2FeO_4 as iron precursors was studied by using a simple pyrolysis technique. The Fe-HTES performance was analyzed by utilizing scanning electron microscopy (SEM), Fourier transform infrared spectroscopy, energy dispersive X-ray spectroscopy, X-ray powder diffraction, Brunauer–Emmett–Teller, and Barrett–Joyner–Halenda (BJH) surface analysis . The effective parameters on the adsorption process such as pH, point of zero charge (pH_{pzc}), initial dye concentration, dose and type of adsorbents raw egg shell (RES), heat treated egg shell (HTES) and Fe-HTES in addition to the adsorption time the dye removal and chemical oxygen demand (COD) removal have been investigated. The results obtained for the dye concentration in the range of 20–100 mg/L, indicated that the experimental adsorption data obeyed the Freundlich model ($n < 1$, $R^2 = 0.981$). At optimum pH 3, the adsorbent dose of 2 g/L and the equilibrium adsorption time of 15 min, the maximum dye removal efficiency were obtained as 98.9%, 88% and 78%, respectively, for Fe-HTES, HTES and RES. For the adsorbent Fe-HTES, the maximum adsorption capacity and COD removal efficiency were obtained as 50 mg/g and 93%, respectively. The results also indicated that the adsorption rate of AR151 dye onto the Fe-HTES can be expressed by a first-order rate equation.

Keywords: Acid red 151 dye; Adsorption; Fe-heat treated egg shell

1. Introduction

Preparation of clean water by removal of hazardous materials is very important from various aspects [1]. Textile dye and colored industrial wastewater contain carcinogenic pollutants such as aromatic amines and toxic pigments and if discharged into rivers and surface streams will endanger the living organisms [2,3].

Various conventional techniques have been employed for the removal of these colored effluents, such as adsorption, oxidation, electrocoagulation and filtration [4]. Adsorption, though might be time consuming, is the most simple, viable and flexible method which has attracted much attention.

Because of using eco-friendly and low cost adsorbents, such as egg shell and plants and availability of adsorbent supports such as saw dust and sugar, efficient adsorption processes have been developed which do not have the obstacles of other removal method [5–7].

Azo dyes are classified as the main dyes which are utilized in various industrial processes [8]. Azo-acid dyes are soluble anionic organic materials and are known by their popular chromogenic azo groups (–N=N–). They are applied to the textile fibers, although approximately 35% of the utilized colors are lost, because they are not fixed to the fabrics and are directly released to textile effluents [9].

* Corresponding author.

Acid red 151 (AR151) is a double azo dye which basically is used for dyeing leather, wool, silk, polyamide fabrics and plastic shading of polyamide. In Table 1, the characteristics of AR151 are represented. To select a biomass such as raw egg shell (RES) for bio-sorption in the dye removal process, some parameters should be taken into account. RES is a calcium carbonate crystal with regular array pattern bio-adsorbent [10,11], however, because of low rigidity, insufficient surface area, small number of active sites it needs to be modified to increase its dye removal efficiency. This adsorbent also should be made immobilize, hard and porous enough, with a reasonable shelf-life during successive regeneration cycles [12,13]. Various composite adsorbents have been synthesized, including magnetic modified chitosan [14] and spinel ferrite [15] for removal of the dyes and pharmaceutical pollutants [16–18].

In this work, surface modification of RSE was performed by thermal treatment and in the presence of three iron precursors $FeCl_2$, $Fe(NO_3)_3$ and K_2FeO_4 in order to improve the uptake and removal capacity of AR151 dye from aqueous solution, by batch adsorption process. Also, the influences of some important operating parameters, such as initial pH, point of zero charge, initial dye concentration, type of adsorbent, adsorbent dose and adsorption time were investigated. Characterization analysis of RSE and the modified bio-adsorbent (Fe-HETS) were performed by using Fourier transform infrared (FTIR), also SEM, energy dispersive X-ray spectroscopy (EDX), X-ray powder diffraction (XRD), Brunauer–Emmett–Teller (BET) and Barrett–Joyner–Halenda (BJH). Also, the adsorption isotherms and the kinetics of the adsorption mechanism were presented by respective models with the best fitted correlation coefficients.

2. Experimental setup

2.1. Materials

All the chemicals were used as the analytical grade reagents. AR151 dye was purchased from Alvan-Sabet company (Iran), and was used without further purification, the chemical structure and other characteristics of AR151 dye are shown in Table 1. $FeCl_2$, $Fe(NO_3)_3 \cdot 9H_2O$ and K_2FeO_4 were of analytical grade as made by Sigma-Aldrich (Germany). Commercial activated carbon (IS 8366:1989) was supplied by Eurocarb (Germany). RES was supplied by the local and campus restaurant of Guilan University (Iran).

Table 1
Characteristics of AR151 dye

Name	Formula	MW (g/g mol)	λ_{max} (nm)
Acid red 151 (AR151)	$C_{22}H_{15}N_4NaO_4S$	454.43	513
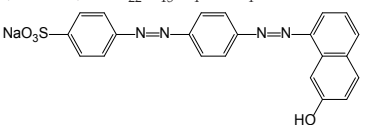
2.2. Preparation of adsorbent – egg shell

RES as an inert porous material with large internal area has high adsorption capacity which can be promoted by using an appropriate modification techniques such as pyrolysis or impregnation with green chemical reagents, namely iron precursors ($FeCl_2$, $Fe(NO_3)_3$ or K_2FeO_4).

In this study, RESs collected from restaurants were washed thoroughly by de-ionized water. The dried RESs were grinded to fine powder and sieved by American Society for Testing and Materials standard sieve, mesh no. 18 (1 mm). Then, the RES was heated for 2 h at 800°C in an electric furnace to obtain the heat treated egg shells (HTESs). The synthesis of Fe-HTES was performed as follows: initially, 5 g of HTES was stirred with 25 mL de-ionized water and 0.5 g of K_2FeO_4 (as strong oxidizing agent to generate active sites on the adsorbent) for 30 min at 150 rpm. The residue or slurry obtained was mixed with 1.5 g $FeCl_2$ and 0.5 g $Fe(NO_3)_3 \cdot 9H_2O$, and stirred for 6 h at 150 rpm and at ambient temperature. The slurry was filtered and washed thoroughly by de-ionized water and decanted and again washed and filtered. Finally, the obtained solid residue was heated at 410°C for 10 min in an electric furnace.

2.3. Methods – batch study

A series of batch adsorption experiments of AR151 dye from aqueous solution using three bio-adsorbents (RES, HTES and Fe-HTES) were tested in a 100 mL flask containing 50 mL of dye solution. Dye removal efficiency percentage was measured based on five different processing factors, including pH (1–11), bio-adsorbent type (RES, HTES and Fe-HTES), dose of bio-adsorbent (0.5–8.0 g/L), initial dye concentration (20–100 mg/L) and the contact time (2–120 min). It was observed that the adsorption equilibrium time was 15 min. The purpose of the adsorption measurements was to determine the optimum operating condition for maximum removal of the dye and chemical oxygen demand (COD) from the test aqueous solutions. All experiments were conducted in triplicates to reduce the error during the tests. The adsorption capacity (q) was determined by using the residual dye concentration before and after adsorption, based on the following material balance equation [4]:

$$q = \frac{C_0 - C_t}{M} v \tag{1}$$

where q is the maximum AR151 dye uptake at equilibrium (mg/g), and C_0 and C_t are the initial and final dye concentrations in the test aqueous solution (mg/L), respectively. In Eq. (1), M is the mass of the adsorbent (in g) and v is the volume of the test dye aqueous solution (in L).

Dye (and also COD) removal efficiency from the test aqueous solution by adsorption was evaluated by using the following equation [4]:

$$\text{Dye removal efficiency } (\%) = \frac{C_0 - C_t}{C_0} \times 100 \tag{2}$$

where the C_0 and C_t are the initial and final dye concentrations (and also initial and final COD). Dye (and also COD) amount before and after adsorption was determined by using

a UV–Vis spectrophotometer (Hach, Lange Model: DR-2800). The absorbance of the dye aqueous solutions was monitored at the wavelength of 200–800 nm and the maximum absorbance was measured at the wavelength of 513 nm. By using these results the required dye concentrations were evaluated. This standard method of concentration measurements for the waste water was the same as used in reference [19]. All the tests were carried out in triplicate and the average value was obtained.

3. Results and discussion

3.1. Adsorbents characterization

3.1.1. SEM analysis of the adsorbents

Scanning electron microscopy (SEM) is a practical tool for investigating the adsorbent particle shape and size distribution. Surface morphological analysis of the RES, HTES and Fe-HTES was performed by using a (VEGA\TESCAN-XMU) SEM, Iran. The SEM images are shown in Figs. 1(a)–(c). Fig. 1(a) indicates an irregular and random treads and strings microstructure configuration for RES. Fig. 1(b) refers to HTES, after 2 h of heat treatment at 800°C, which shows that the adsorbent surface is ordered as an ideal knitted treads with regular square voids, that has been created during the CO_2 removal [11], where the formation of this microstructure can be attributed to the presence of calcium oxide [20]. Fig. 1(c) shows a clear image of numerous micropores present on the surface of Fe-HTES agglomerates, as created by the addition of three iron reagents. It is seen that, the pore sizes of this chemically modified calcium oxide sample are smaller than 1 μm. These images indicate clearly that the microstructure of the eggshell particles (with and without modification) changes in size and shape, as a result of heat treatment.

3.1.2. EDX analysis of the adsorbents

EDX analysis of HTES and Fe-HTES are shown in Figs. 2(a) and (b). Fig. 2(a) indicates that the weight percentage of C, O and Ca in HTES are, respectively, 13.3, 39 and 46.6, and the ratio of Ca:O is 1:1 which confirms the presence of calcium oxide (CaO), as a result of egg shell calcination at 800°C in 2 h. Fig. 2(b) shows that the weight percentage of C, N, O, Cl, K, Ca and Fe in Fe-HTES which are, respectively, 2, 6.4, 37.1, 4, 0.4, 50.4 and 7.

3.1.3. FTIR analysis of the adsorbents

In this study, FTIR spectroscopy method was utilized to investigate the presence of functional groups on the surface of the egg shell. FTIR spectra (by a PerkinElmer spectrometer) for three adsorbents (RES, HTES and Fe-HTES) in the range 4,000–450 cm^{-1} were obtained and are depicted in Figs. 3(a)–(c). The three characteristic peaks which are at 3,431, 3,447 and 3,524 cm^{-1} in RES, HTES are due to an OH group as suggested by other researchers [20–22]. In the RES (containing 94% $CaCO_3$, 1% $MgCO_3$, 1% $Ca_3(PO_4)_2$ and 4% organic material [23]), the two characteristic peaks appearing at 2,516 and 1,420 cm^{-1} can be attributed to the presence of $CaCO_3$ as proposed by Legodi et al. [24] and Arnold et al. [25]. However, after calcinations of RES and obtaining HTES or Fe-HTES these peaks have disappeared, which is due to decomposition of $CaCO_3$ at 800°C and production of CaO and CO_2. The new slightly sharp peaks at 3,642 cm^{-1} for HTES and
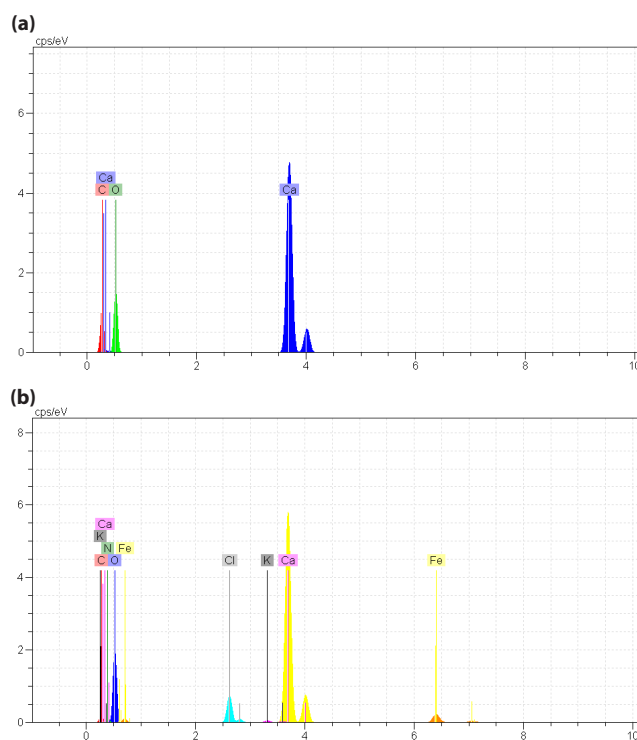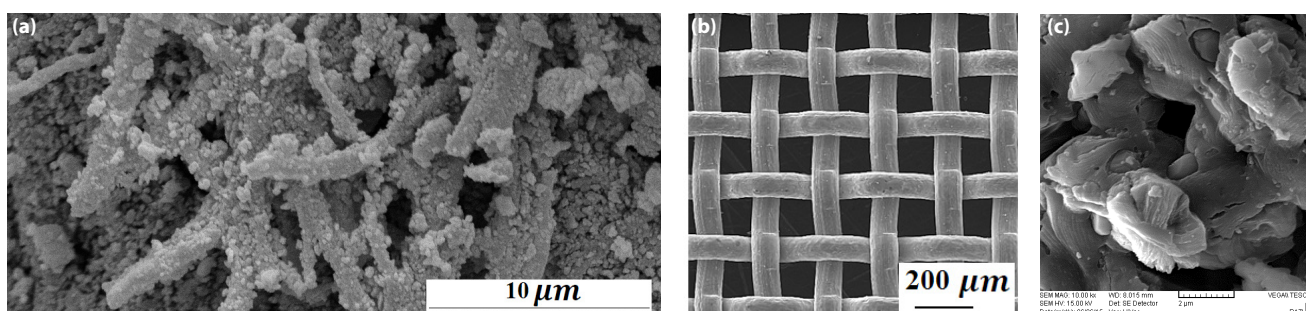

Fig. 2. EDX of: (a) HTES and (b) Fe-HTES.

Fig. 1. SEM image of three adsorbents: (a) raw eggshell (RES), (b) heat treated egg shell (HTES) and (c) iron-impregnated heat treated egg shell (Fe-HTES).
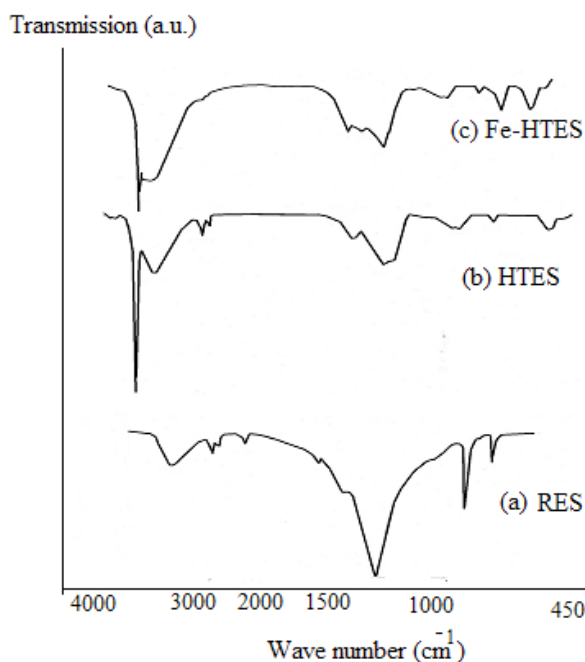
Fig. 3. FTIR spectra before adsorption of: (a) RES, (b) HTES and (c) Fe-HTES.

Fig. 4. XRD diffractogram of Fe-HTES adsorbent.

$$D = \frac{k\lambda}{\beta \mathrm{Cos}\theta} \tag{3}$$

where β (rad) is the full width at half of the maximum height, $k = 0.9$ is a dimensionless constant, θ is the Bragg angle. The minor phases are calcium oxide (CaO) [32,34], calcium carbonate hydroxide ($Ca_3(CO_3)_2(OH)_2$) [35–37] and Fe_2O_3 [18,38–40] that they refer to complete combustion of RES at 800°C. The presence of Fe_2O_3 and ($Ca_3(CO_3)_2(OH)_2$) are, respectively, due to iron precursors ($FeCl_2$, Fe ($NO_3)_3$ or K_2FeO_4) [18,38–40] and portlandite decomposition [30,32,34,36].

3.1.5. Surface analysis of the Fe-HTES adsorbent

The specific surface area of the Fe-HTES was determined as 89.97 (m^2/g) by BET method using the Quantachrome Autosorb (Germany). The BET adsorption–desorption isotherms of nitrogen gas at low temperature [29] and in the relative pressure range of $0.1 < P/P_0 < 0.3$ is represented in Fig. 5. The observed hysteresis of this isotherm plot confirms the presence of Fe-HTES as a mesoporous adsorbent (type IV of the International Union of Pure and Applied Chemistry rank) [41]. The total pore volume for the presence of pores smaller than 2.62 nm as obtained by BET method at $P/P_0 = 0.30608$ is 0.02536 mL/g. The surface area, the pore size and volume were calculated by BJH [42] method using the data obtained by adsorption measurements (Quantachrome Autosorb, Germany). The obtained results are, respectively, 110.5 m^2/g, 5.695 nm and 0.315 mL/g for the specific surface area, pore size and volume.

Inspecting XRD, BET, SEM, EDX and FTIR results obtained in this work indicate the presence of hydroxyl functional group and oxygen bridges in the major and minor phases of Fe-HTES and this confirms the existence of hydrogen bonds and the presence of various active points in the adsorbent molecule. Therefore, the adsorption capacity of this adsorbent is essentially due to the presence of various effective sites [16–18,43] arisen by iron impregnation [44], and other heteroatom as is seen in Fig. 2. Also, the maximum dye removal efficiency for Fe-HTES adsorbent occurred at pH < 3 and this indicates the presence of adequate positive charges on the surfaces of highly crystallite portlandite as the major phase [45] which introduces this adsorbent desirable for adsorption of anionic acid dye due to electrostatic interactions. The electronic density of the adsorbents' layers and the presence of hydroxyl functional group attract the dye into the surface [46]. Due to nature of the physical bonds in the adsorption process the Fe-HTES adsorbents can be properly separated from an aqueous dye solution after adsorption process by applying filtration [16,17].

3,643.5 cm^{-1} for Fe-HTES correspond to CaO as suggested by Arnold et al. [25] and the other new bands at 1,466 cm^{-1} for HTES and 1,416 cm^{-1} for Fe-HTES, also correspond to the presence of CaO as suggested by Zaki et al. [26]. Another band at 660 cm^{-1} can be assigned to CaO too, as explained by Witoon [22]. Consequently, FTIR findings demonstrate that $CaCO_3$ has transformed to CaO in the pyrolized HTES and Fe-HTES. In Fe-HTES, the new band at 872 cm^{-1} corresponds to the presence of Fe–OH or metal–oxygen bond as proposed by Liu et al. [27], hence in the FTIR spectrum of RES and HTES this band is not present.

The point of zero charge (which is also represented as pH_{pzc}) plays a substantial role in adsorption of an ionic adsorbate from aqueous solution on a solid adsorbent. The pH_{pzc} is defined as the pH value when the solid surface is neutral. The point of zero charge can be utilized to evaluate the electrical charge of solid adsorbent. In this study for pH_{pzc} measurements, the procedure previously reported, by other researchers was used [28]. The pH_{pzc} values for the three adsorbents Fe-HTES, HTES and RES occurred at the approximate pHs of 3.2, 4.5 and 5.1, respectively.

3.1.4. XRD analysis of the Fe-HTES adsorbent

In this study, to investigate the structural characteristics of the obtained Fe-HTES the XRD (Philips, PW1800, Netherland) analyses was performed by using a voltage of 40 kV and a current of 30 mA with Cu Kα radiation (X-ray wavelength, $\lambda = 0.1542$ nm). The X-ray pattern is demonstrated in Fig. 4. The major peak in the XRD pattern which appears at $2\theta = 34.08°$, corresponds to the presence of portlandite (Ca(OH)$_2$) as the major phase [29–32]. The crystallite size ($D = 45$ nm) of this major phase can be calculated by Scherer's equation [33]:

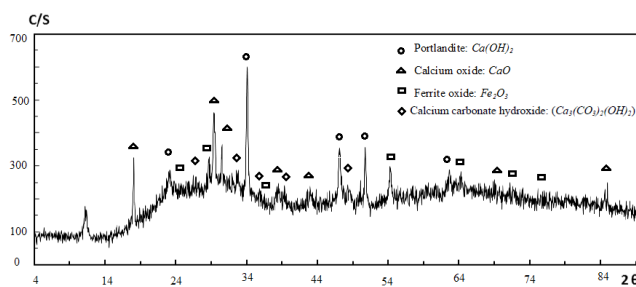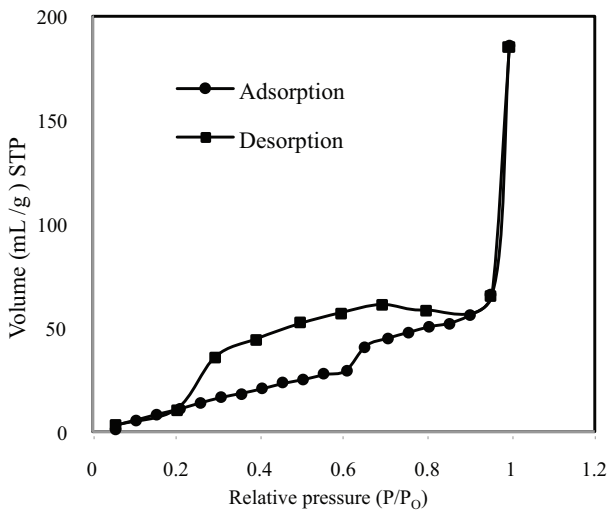Fig. 5. Volume (at standard temperature and pressure (STP) of nitrogen gas adsorption/desorption on Fe-HTES surface vs. nitrogen relative pressure (P/P_0) by BET method.

3.2. Effect of operational parameter on dye removal

3.2.1. Effect of pH

The pH of the dye solution is a significant factor that regulates the adsorption process. To study the effect of initial pH on the adsorption, the AR151 dye solution pH was varied from 1 to 11 and the results for the adsorbent Fe-HTES are presented in Fig. 6. The minimum residual dye concentration was reduced to 1 mg/L (maximum dye removal efficiency 98%) at pH 1–3. But at higher pHs the residual dye concentration was 13 mg/L at pH 11. Consequently, the removal efficiency percentage and adsorption capacity for pH variation 1–11 were 99% to 87% and 50 to 43.5 mg/g, respectively. The reason for this behavior can be explained by considering the fact that at the pH < 3 the surface of Fe-HTES is positively charged which is suitable for binding of negatively charged AR151 dye. This interpretation of the obtained results for pH effect is confirmed by reported results on higher tendency of AR151 dye and adsorption on Fe-HTES due to electrostatic attraction at pH less than pH_{pzc} [28,47,48]. Also, it has been observed that at acidic pH the adsorption of acid type dyes (acid red 114, acid blue 113, acid green 28, etc.) is more favorable [47].

3.2.2. Effect of adsorbent dosage

Fig. 7 shows that the residual AR151 dye concentration decreases gradually to a minimum (2 g/L) with increasing Fe-HTES adsorbent concentration (up to 6 g/L) and then on addition of Fe-HTES no more reduction of AR151 dye is observed which indicates that the system has reached the equilibrium state.

3.2.3. Effect of initial AR151 dye concentration and adsorbent type

The effect of initial AR151 dye concentration on adsorption capacity (Eq. (1)) of three studied adsorbents, Fe-HTES, HTES and RES, and also commercial activated carbon were
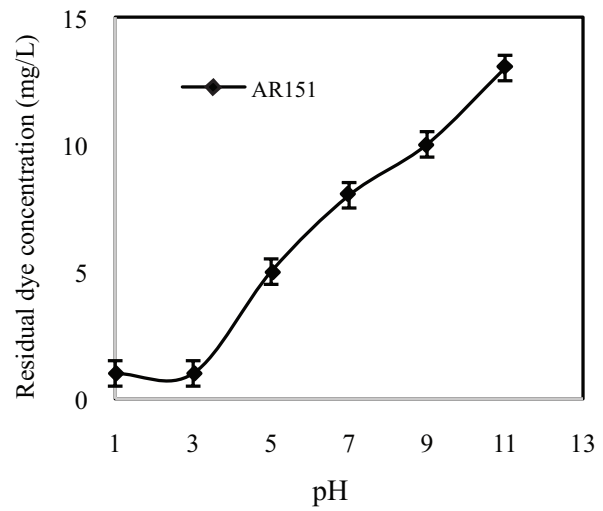

Fig. 6. Effect of pH on the AR151 dye residual concentration (initial dye concentration, 100 mg/L; adsorption equilibrium time, 15 min; dose of adsorbent, 2 g/L; adsorbent, Fe-HTES; initial volume of working dye solution, 50 mL; dye removal efficiency, 98.9%).
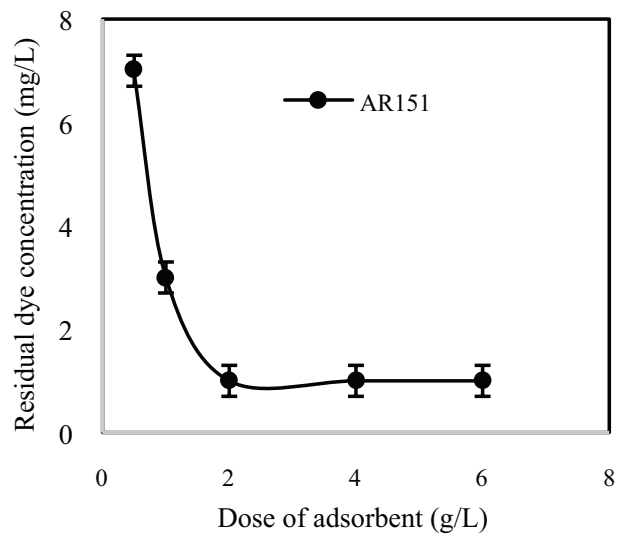

Fig. 7. Effect of the adsorbent dosages on the residual dye concentration (pH, 3; initial dye concentration, 100 mg/L; adsorption equilibrium time, 15 min; adsorbent, Fe-HTES; initial volume of working dye solution, 50 mL; dye removal efficiency, 98.9%).

investigated. The comparison of the AR151 dye adsorption capacity is summarized in Fig. 8 which indicates that by increasing the initial dye concentration from 20 to 100 mg/L, the adsorption capacity increases. Based on Eq. (1) and by inspecting this figure it is seen that the highest adsorption capacity (50, 44 and 39 mg/g are, respectively, for Fe-HTES, HTES and RES) occurs at 100 mg/L of the dye concentration for the three adsorbents. It can be stated that the adsorption process for the four adsorbents has reached the equilibrium state (pH, 3; adsorption equilibrium time, 15 min; initial volume of working dye solution, 50 mL; dose of adsorbent, 2 g/L) at each certain dye concentration. Additionally, by
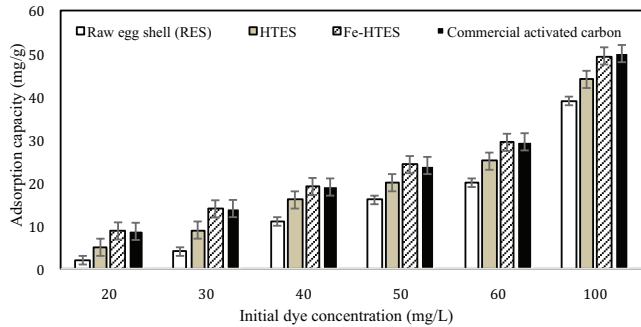
Fig. 8. Comparison of the effect of initial AR151 dye concentration on adsorption capacity of four adsorbents (pH, 3; adsorption equilibrium time, 15 min; initial volume of working dye solution, 50 mL; dose of adsorbent, 2 g/L).

using Eq. (2) and as it is indicated from the data of Fig. 8, the highest dye removal efficiency are 78%, 88%, 98.9% and 98.9%, respectively, for Fe-HTES, HTES, RES and commercial activated carbon. Therefore, it can be stated that Fe-HTES and also commercial activated carbon can effectively remove the AR151 dye from aqueous solution compared with the two other adsorbents. These results are consistent with the reported results by other researchers for the adsorption of dyes on bio-adsorbents [49,50].

3.3. Adsorption isotherms determination

The isotherm models are good description of adsorption process and provide useful information [51–55]. Therefore, the experimental data were fitted by the some well known isotherm models such as Langmuir, Freundlich and Temkin equations.

The Langmuir equation is in the following form [52]:

$$\frac{C_e}{q_e} = \frac{1}{q_m b} + \frac{C_e}{q_m} \tag{4}$$

where C_e (mg/L) is the residual dye concentration in the aqueous solution at equilibrium, q_e (mg/g) and q_m (mg/g) are, respectively, the equilibrium and maximum adsorption capacities. In Eq. (4), b (L/mg) is the Langmuir constant and is interpreted as the free energy of adsorption. The constants q_m and b are evaluated by the slope and intercept of the plot C_e/q_e vs. C_e. The adsorption results as treated by Eq. (4) are reported in Table 2.

Linear form of Freundlich equation is [53]:

$$\log q_e = \log K_F + \frac{1}{n}\log C_e \tag{5}$$

where K_F (mg/g) is adsorption capacity at unit concentration and $1/n$ is the adsorption intensity of bond formation between the dye molecule and the adsorbent, n is dimensionless quantity. It has been demonstrated that for the values of n less than 10 and greater than zero, there is the favorable adsorption. K_F and n can be calculated by plotting $\log q_e$ vs. $\log C_e$. For $n = 1$, the adsorption is linear and for $n > 1$ it is a physisorption process and for $n < 1$, it is a chemisorption

Table 2
Isotherm constants of three linearized adsorption isotherms for AR151 dye adsorption onto Fe-HTES adsorbent (K_F: mg/g; K_T: L/mg; B_1: mg/g; q_m: mg/g and b: L/mg)

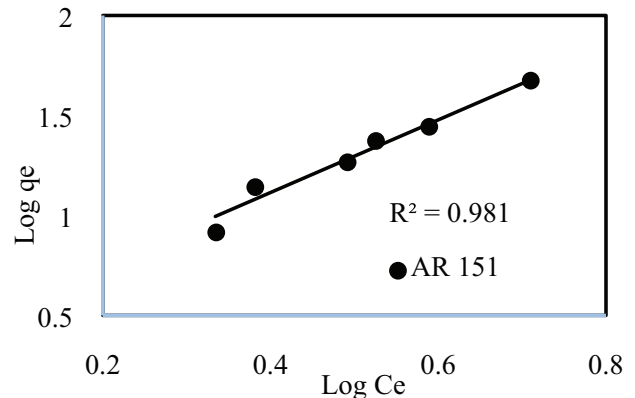| Dye	Freundlich			Temkin			Langmuir		
	n	K_F	R^2	B_1	K_T	R^2	q_m	b	R^2
AR151	0.55	2.44	0.981	6.86	2.7	0.89	14	0.40	0.56

Fig. 9. Freundlich plot of AR151 dye adsorption onto Fe-HTES at different initial dye concentrations (pH, 3; adsorption equilibrium time, 15 min; initial volume of working dye solution, 50 mL; dose of adsorbent, 2 g/L).

process [54]. The adsorption results as treated by Eq. (5) are presented in Fig. 9 and Table 2.

Linear form of the Temkin equation is presented as [55]:

$$q_e = B_1 \ln K_T + B_1 \ln C_e \tag{6}$$

where $B_1 = \frac{RT}{a}$ K_T (L/mg) is the maximum binding energy (or equilibrium binding constant) and B_1 is a constant corresponding to the heat of adsorption. Temkin constants K_T and B_1 are calculated from the slope and intercept of the plot $\log q_e$ vs. $\log C_e$.

The R^2 values show that the AR151 dye adsorption isotherm using the adsorbent Fe-HTES does not follow the Langmuir and Temkin isotherms (Table 2). Fig. 9 shows the linear plot of $\log q_e$ vs. $\log C_e$ for the Freundlich equation. The calculated values for this equation are: R^2 (0.981), n (0.55) and K_F (2.44 mg/L) at optimum conditions (pH 3, dose of adsorbent 2 g/L) which represent the suitability of this equation for the obtained adsorption results.

The equilibrium measurement was performed for different initial AR151 dye concentration (20–100 mg/L) subsequently the adsorption capacity (evaluated by Eq. (1)) of Fe-HTES was varied from 8.9 to 50 mg/g. It seems that Freundlich equation is suitable for treating the dye removal by adsorption. As an example, the adsorption results obtained by Nekouei et al. [56], can be quoted which are in accord with the Freundlich equation and the evaluated parameters for the adsorption of acid blue 129 on 0.8 g/L

copper oxide activated carbon at pH = 2 after 20 min were K_F = 31.35 mg/L and n = 4.

3.4. Kinetics of adsorption

For determining the most appropriate adsorption rate model, the adsorption results were fitted to the first- and second-order rate equations, for the measured removal efficiency of AR151 by Fe-HTES vs. time. The rate equations, first- and second-order are, respectively, expressed by Eqs. (7) and (8) [52,53] in the following forms:

$$\log\left(q_e - q_t\right) = \log q_e - k_1 t \tag{7}$$

$$\left(\frac{t}{q_t}\right) = \left(\frac{1}{\left(k_2 q_e^2\right)}\right) + \left(\frac{1}{q_e}\right)t \tag{8}$$

where q_t (mg/g) is the amount of dye uptake per unit weight of the adsorbent (Fe-HTES) at equilibrium, q_e (mg/g) is the amount of dye uptake per unit weight of Fe-HTES adsorbent at t and k_1 (1/min) and k_2 (g/(mg.min)) are the rate constants of the first- and second-order rate models, respectively. q_e and k_1 were calculated from the slope and intercept of the plot $\log(q_e - q_t)$ vs. t by Eq. (7). q_e and k_2 were calculated from the slope and intercept of the plot (t/q_t) vs. t by Eq. (8). The results are presented in Table 3 and Fig. 10 (R^2 = 0.983 for the first-order model).

Table 3
Calculated kinetic parameters for the adsorption of AR151 dye onto Fe-HTES adsorbent (q_e: mg/g; k_1: 1/min; k_2: g/(mg.min) and q_{exp}: mg/g)

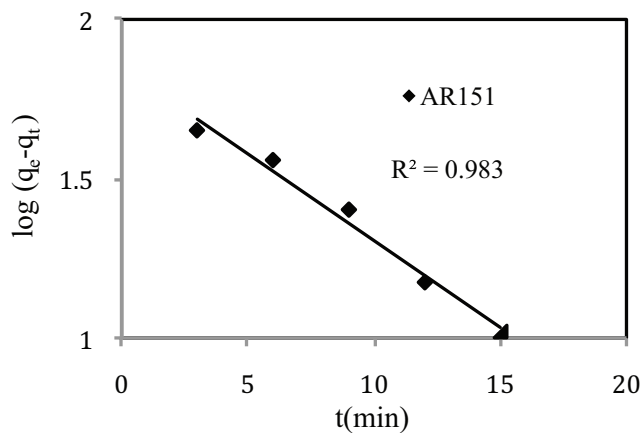| Dye	Pseudo-First-order model				Pseudo-second-order model		
	q_{exp}	q_e	k_1	R^2	q_e	k_2	R^2
AR151	49.5	50	0.054	0.983	142	0.0003	0.880

Fig. 10. Linearized first-order kinetic plot for AR151 dye adsorption by Fe-HTES (initial dye concentrations, 100 mg/L; pH, 3; initial volume of working dye solution, 50 mL; dose of adsorbent, 2 g/L).

This implies that the first-order model is more appropriate to describe the kinetics of AR151 adsorption on Fe-HTES with the rate constant k_1 = 0.054 (1/min).

A similar work mentioned is that of Jafari et al. [57] who showed that adsorption of methylene blue dye on the modified TiO_2 adsorbent followed the pseudo-first-order kinetic model with k_1 = 0.004(1/min).

3.5. COD removal efficiency percentage

In this study, COD procedure is utilized to measure the amount of organic pollutants such as dye in water. The COD analysis was performed according to the standard procedure of 5220B [19,58]. A COD experiment was performed by applying the optimized operating factors with regard to different variables obtained for uptake of AR151 by Fe-HTES. The optimum conditions were: initial dye concentrations, 100 mg/L; pH, 3; initial volume of the test dye solution, 50 mL; type and the dose of adsorbent, Fe-HTES 2 g/L and after equilibrium time (15 min). The COD removal efficiency and the dye removal efficiency were evaluated by Eq. (2) as 93% and 98.9%, respectively. However, the COD removal efficiency by Eq. (2) for RES and HTES adsorbents were 65% and 75%, respectively. This difference could be attributed to the presence of potassium ferrate (K_2FeO_4) as a strong oxidizing precursor for Fe-HTES [59].

4. Conclusions

Bio-adsorbent Fe-HTES was synthesized and its ability for removal of AR151 dye aqueous solution was evaluated (98.9%), the effectiveness of Fe-HTES was compared with the RES and HTES. The results indicated that the Fe-HTES had the maximum adsorption capacity of 50 mg/g. Maximum AR151 dye removal appeared at pH 3 and during 15 min of the equilibrium time and the optimum dosage of Fe-HTES was 0.2 g. However, at COD removal efficiency of 93% the mineralization occurred. Adsorbent characteristics were examined by FTIR, EDX, XRD, BET and SEM and the results confirmed that $CaCO_3$ had properly transformed to portlandite ($Ca(OH)_2$) in the pyrolized egg shells. The adsorption results followed both Freundlich isotherm equation and first-order kinetic model.

References

[1] N.G. Vaquero, E. Lee, R.J. Castañeda, J. Cho, J.A. López-Ramírez, Comparison of drinking water pollutant removal using a nanofiltration pilot plant powered by renewable energy and a conventional treatment facility, Desalination, 347 (2014) 94–102.

[2] B. Bakheet, S. Yuan, Z.X. Li, H.J. Wang, J.N. Zuo, S. Komarneni, Y. Wang, Electro-peroxone treatment of orange II dye wastewater, Water Res., 47 (2013) 6234–6243.

[3] T.S. Anantha Singh, S. Thanga Ramesh, An experimental study of CI reactive blue 25 removal from aqueous solution by electrocoagulation using aluminum sacrificial electrode: kinetics and influence of parameters on electrocoagulation performance, Desal. Wat. Treat., 52 (2014) 2634–2642.

[4] V.K. Gupta, Suhas, Application of low-cost adsorbents for dye removal – a review, J. Environ. Manage., 90 (2009) 2313–2342.

[5] S. Chowdhury, P. Saha, Sea shell powder as a new adsorbent to remove basic green 4 (malachite green) from aqueous solutions: equilibrium, kinetic and thermodynamic studies, Chem. Eng. J., 164 (2010) 168–177.

[6] H. Daraei, A. Mittal, M. Noorisepehr, J. Mittal, Separation of chromium from water samples using eggshell powder as a low-cost sorbent: kinetic and thermodynamic studies, Desal. Wat. Treat., 53 (2015) 214–220.

[7] S. Chowdhury, S. Chakraborty, P. Saha, Biosorption of basic green 4 from aqueous solution by *Ananas comosus* (pine apple) leaf powder, Colloids Surf., B, 84 (2011) 520–527.

[8] W. Feng, D. Nansheng, H. Helin, Degradation mechanism of azo dye C. I. Reactive red 2 by iron powder reduction and photooxidation in aqueous solutions, Chemosphere, 41 (2000) 1233–1238.

[9] S. Wijetung, L. Xiufen, R. Wenquan, Removal mechanisms of acid dyes of different chemical groups under anaerobic mixed culture. Ruhuna J. Sci., 2 (2007) 96–100.

[10] W.T. Tsai, J.M. Yang, H.C. Hsu, C.M. Lin, K.Y. Lin, C.H. Chiu, Development and characterization of mesoporosity in eggshell ground by planetary ball milling, Microporous Mesoporous Mater., 111(2008) 379–386.

[11] Z. Wei, C. Xu, B. Li, Application of waste eggshell as low-cost solid catalyst for biodiesel production, Bioresour. Technol., 100 (2009) 2883–2885.

[12] W.T. Tsai, K.J. Hsien, H.C. Hsu, K.Y. Lin, C.H. Chiu, Utilization of ground eggshell waste as an adsorbent for the removal of dyes from aqueous solution. Bioresour. Technol., 6 (2008) 1623–1629.

[13] H.K. Alluri, S.R. Ronda, V.S. Settalluri, J.S. Bondili, V. Suryanarayana, P. Venkateshwar, Biosorption: An eco-friendly alternative for heavy metal removal, Afr. J. Biotechnol., 25 (2007) 2924–2931.

[14] K. Li, P. Li, J. Cai, S. Xiao, H. Yang, A. Li, Efficient adsorption of both methyl orange and chromium from their aqueous mixtures using a quaternary ammonium salt modified chitosan magnetic composite adsorbent, Chemosphere, 154 (2016) 310–318.

[15] D.H. Kumar Reddy, Y.S. Yun, Spinel ferrite magnetic adsorbents: alternative future materials for water purification?, Coord. Chem. Rev., 315 (2016) 90–111.

[16] S. Wang, M. Ma, Q. Zhang, G. Sun, T. Jiao, R.K. Okazaki, Efficient phosphate sequestration in waters by the unique hierarchical 3D *Artemia* egg shell supported nano-Mg(OH)$_2$ composite and sequenced potential application in slow release fertilizer, ACS Sustain. Chem. Eng., 3 (2015) 2496–2503.

[17] H. Guo, T. Jiao, Q. Zhang, W. Guo, Q. Peng, X. Yan, Preparation of graphene oxide-based hydrogels as efficient dye adsorbents for wastewater treatment, Nanoscale Res. Lett., 10 (2015) 1–10. doi: 10.1186/s11671-015-0931-2.

[18] W. Wang, T. Jiao, Q. Zhang, X. Luo, J. Hu, Y. Chen, Q. Peng, X. Yan, B. Li, Hydrothermal synthesis of hierarchical core–shell manganese oxide nanocomposites as efficient dye adsorbents for wastewater treatment, RSC Adv., 5 (2015) 56279–56285.

[19] APHA, AWWA, WPCF, Standard Methods for the Examination of Water and Wastewater, 21st ed., American Public Health Association, Washington, D.C., 2005.

[20] E. Mosaddegh, A. Hassankhani, Preparation and characterization of nano-CaO based on eggshell waste: novel and green catalytic approach to highly efficient synthesis of pyrano[4,3-b] pyrans, Chin. J. Catal., 3 (2014) 351–356.

[21] V. Michel, Ph. Ildefonse, G. Morin, Assessment of archaeological bone and dentine preservation from Lazaret cave (Middle Pleistocene) in France, Palaeogeogr. Palaeoclimatol. Palaeoecol., 126 (1996) 109–119.

[22] T. Witoon, Characterization of calcium oxide derived from waste eggshell and its application as CO_2 sorbent, Ceram. Int., 37 (2011) 3291–3298.

[23] S. Lunge, D. Thakre, S. Kamble, N. Labhsetwar, S. Rayalu, Alumina supported carbon composite material with exceptionally high defluoridation property from eggshell waste, J. Hazard. Mater., 237–238 (2012) 161–169.

[24] M.A. Legodi, D. de Waa1, J.H. Potgieter, S.S. Potgieter, Rapid determination of CaCO$_3$ in mixtures utilizing FTIR spectroscopy, Miner. Eng., 14 (2001) 1107–1111.

[25] T. Arnold, M. Rozario-Ranasinghe, J. Youtcheff, Determination of lime in hot mix asphalt, Transp. Res. Rec., 1962 (2006) 113–120.

[26] M.I. Zaki, H. Knozinger, B. Tesche, G.A.H. Mekhemer, Influence of phosphonation and phosphation on surface acid–base and morphological properties of CaO as investigated by in situ FTIR spectroscopy and electron microscopy, J. Colloid Interface Sci., 303 (2006) 9–17.

[27] J.Y. Liu, S.P. Wang, J.M. Yang, J.J. Liao, M. Lu, H.J. Pan, L. An, ZnCl$_2$ activated electrospun carbon nanofiber for capacitive desalination, Desalination, 344 (2014) 446–453.

[28] P.C.C. Faria, J.J.M. Órfão, M.F.R. Pereira, Adsorption of anionic and cationic dyes on activated carbons with different surface chemistries, Water Res., 38 (2004) 2043–2052.

[29] R. Chakraborty, S. Bepari, A. Banerjee, Transesterification of soybean oil catalyzed by fly ash and egg shell derived solid catalysts, Chem. Eng. J., 165 (2010) 798–805.

[30] M. Cyr, M. Trinh, B. Husson, G. Casaux-Ginestet, Effect of cement type on metakaolin efficiency, Cem. Concr. Res., 64 (2014) 63–72.

[31] A.M. Kalinkin, E.V. Kalinkina, O.A. Zalkind, T.I. Makarova, Chemical interaction of calcium oxide and calcium hydroxide with CO_2 during mechanical activation, Inorg. Mater., 41 (2005) 1073–1079.

[32] Y.H. Tan, M.O. Abdullah, C. Nolasco-Hipolito, Y.H. Taufiq-Yap, Waste ostrich- and chicken-eggshells as heterogeneous base catalyst for biodiesel production from used cooking oil: catalyst characterization and biodiesel yield performance, App. Energy, 160 (2015) 58–70.

[33] H. Klug, L. Alexander, X-ray Diffraction Procedures, John Wiley and Sons Inc., New York, 1962.

[34] B. Derkus, Y.E. Arslan, K.C. Emregul, E. Emregul, Enhancement of aptamer immobilization using egg shell-derived nano-sized spherical hydroxyapatite for thrombin detection in neuroclinic, Talanta 158 (2016) 100–109.

[35] E.T. Stepkowska, Simultaneous IR/TG study of calcium carbonate in two aged cement pastes, J. Therm. Anal. Calorim., 84 (2006) 175–180.

[36] W.P. Li, V. Shanmugam, C.C. Huang, G.D. Huang, Y.K. Huang, S.H. Chiu, C.S. Yeh, Eccentric inorganic-polymeric nanoparticles formation by thermal induced cross-linked esterification and conversion of eccentricity to raspberry-like Janus, Chem. Commun., 49 (2013) 1609–1611.

[37] E.T. Stepkowska, Hypothetical transformation of Ca(OH)$_2$ into CaCO$_3$ in solid-state reactions of Portland cement, J. Therm. Anal. Calorim., 80 (2005) 727–733.

[38] E. Kılınç, γ-Fe$_2$O$_3$ magnetic nanoparticle functionalized with carboxylated multi walled carbon nanotube: synthesis, characterization, analytical and biomedical application, J. Magn. Magn. Mater., 401 (2016) 949–955.

[39] N.G. Sahoo, H. Bao, Y. Pan, M. Pal, M. Kakran, H.K.F. Cheng, L. Li, L.P. Tan, Functionalized carbon nanomaterials as nanocarriers for loading and delivery of a poorly water-soluble anticancer drug: a comparative study, Chem. Commun., 47 (2011) 5235–5237.

[40] H. Jiao, J. Wang, Single crystal ellipsoidal and spherical particles of α-Fe$_2$O$_3$: hydrothermal synthesis, formation mechanism, and magnetic properties, J. Alloys Compd., 577 (2013) 402–408.

[41] K.S.W. Sing, D.H. Everett, R.A.W. Haul, L. Moscou, R.A. Pierotti, J. Rouquerol, T. Siemieniewska, Reporting physisorption data for gas/solid systems with special reference to the determination of surface area and porosity (recommendations 1984), Pure Appl. Chem., 57 (1985) 603–619.

[42] E.P. Barret, L.G. Joyner, P.H. Halenda, The determination of pore volume and area distributions in porous substances. 1. Computations from nitrogen isotherms, J. Am. Chem. Soc., 73 (1951) 373–380.

[43] M.A. Al-Ghouti, Y.S. Al-Degs, F.I. Khalili, Minimisation of organosulphur compounds by activated carbon from commercial diesel fuel: Mechanistic study, Chem. Eng. J., 162 (2010) 669–676.

[44] Y. Liu, G. Su, B. Zhang, G. Jiang, B. Yan, Nanoparticle-based strategies for detection and remediation of environmental pollutants, Analyst 136 (2011) 872–877.

[45] C. Namasivayam, D. Kavitha, Removal of Congo Red from water by adsorption onto activated carbon prepared from coir pith, an agricultural solid waste, Dyes Pigm., 54 (2002) 47–58.

[46] L.R. Radovic, C. Moreno-Castilla, J. Rivera-Utrilla, Carbon Materials as Adsorbents in Aqueous Solutions, L.R. Radovic, Ed., Chemistry and Physics of Carbon, Marcel Dekker, New York, 2001, pp. 227–405.

[47] M. Anbia, S. Salehi, Removal of acid dyes from aqueous media by adsorption onto amino-functionalized nanoporous silica SBA-3, Dyes Pigm., 94 (2012) 1–9.

[48] I. Shah, R. Adnan, W.S. Wan Ngah, N. Mohamed, Iron impregnated activated carbon as an efficient adsorbent for the removal of methylene blue: regeneration and kinetics studies, PLoS ONE 10 (2015) 1–23. doi: 10.1371/journal.pone.0122603.

[49] A.K. Kushwaha, N. Gupta, M.C. Chattopadhyaya, Removal of cationic methylene blue and malachite green dyes from aqueous solution by waste materials of *Daucus carota*, J. Saudi Chem. Soc., 18 (2014) 200–207.

[50] A. Mittal, J. Mittal, A. Malviya, V.K. Gupta, Adsorptive removal of hazardous anionic dye "Congo red" from wastewater using waste materials and recovery by desorption, J. Colloid Interface Sci., 340 (2009) 16–26.

[51] L. Ai, Y. Zeng, J. Jiang, Hierarchical porous BiOI architectures: facile microwave non-aqueous synthesis, characterization and application in the removal of Congo red from aqueous solution, Chem. Eng. J., 235 (2014) 331–339.

[52] L. Zhou, J. Huang, B. He, F. Zhang, H. Li, Peach gum for efficient removal of methylene blue and methyl violet dyes from aqueous solution, Carbohydr. Polym., 101 (2014) 574–581.

[53] A. Mittal, D. Jhare, J. Mittal, Adsorption of hazardous dye Eosin Yellow from aqueous solution onto waste material de-oiled soya: isotherm, kinetics and bulk removal, J. Mol. Liq., 179 (2013) 133–140.

[54] N.K. Amin, Removal of reactive dye from aqueous solutions by adsorption onto activated carbons prepared from sugarcane bagasse pith, Desalination, 223 (2008) 152–161.

[55] M. Ghaedi, K. Mortazavi, M. Montazerozohori, A. Shokrollahi, M. Soylak, Flame atomic absorption spectrometric (FAAS) determination of copper, iron and zinc in food samples after solid-phase extraction on Schiff base-modified duolite XAD 761, Mater. Sci. Eng., C, 33 (2013) 2338–2344.

[56] F. Nekouei, S. Nekouei, I. Tyagi, V.K. Gupta, Kinetic thermodynamic and isotherm studies for acid blue 129 removal from liquids using copper oxide nanoparticle-modified activated carbon as a novel adsorbent, J. Mol. Liq., 201 (2015) 124–133.

[57] S. Jafari, F. Zhao, D. Zhao, M. Lahtinen, A. Bhatnagar, M. Sillanpää, A comparative study for the removal of methylene blue dye by N and S modified TiO_2 adsorbents, J. Mol. Liq., 207 (2015) 90–98.

[58] E. Keshmirizadeh, H. Modarress, R. Didehkhani, The fast decolorization of reactive red 31 (RR31) dye solution by ceric ammonium nitrate (CAN), Desal. Wat. Treat., 57 (2016) 12274–12280.

[59] C. Wu, L. Jin, P. Zhang, G. Zhang, Effects of potassium ferrate oxidation on sludge disintegration, dewaterability and anaerobic biodegradation, Int. Biodeterior. Biodegrad., 102 (2015) 137–142.